RSC Advances

PAPER

Cite this: *RSC Adv.*, 2016, **6**, 72386

Conformational analysis of bovine serum albumin adsorbed on halloysite nanotubes and kaolinite: a Fourier transform infrared spectroscopy study†

Valentina Della Porta,[a] Emilia Bramanti,*[a] Beatrice Campanella,[ab] Maria Rosaria Tiné[b] and Celia Duce[b]

Received 13th May 2016
Accepted 22nd July 2016

DOI: 10.1039/c6ra12525e

www.rsc.org/advances

Clay minerals are widely used in pharmaceutical formulations, therefore studying how they interaction with proteins is important because they can alter their biological functions. The interactions of proteins with nanostructured clays and, in general, with nanomaterials should also be studied because nanoparticles are known to interfere with protein amyloid formation, which is implicated in severe neurodegenerative diseases. Kaolinite and halloysite belong to the kaolinite group of minerals with the nominal formula $Al_2Si_2O_5(OH)_4$ per half unit cell, however they have important structural layer stacking differences. We studied the surface interactions between clays and bovine serum albumin (BSA) by Fourier Transform Infrared Spectroscopy in order to understand the role of clay morphology on protein conformation. We show that the conformational changes of BSA depend on protein concentration and its initial structure, clay morphology and the clay/protein ratio. The surface curvature radius seems to play a key role in the final conformation. Both the curved nanoscale surface of halloysite nanotubes (HNTs) and the flat morphology of kaolinite (Kao) interfere profoundly on the α/β transitions of BSA. BSA conformation also determines the percentage of protein adsorbed on the clay surface.

1. Introduction

The adsorption and binding of protein molecules by clay minerals play key roles in many biological applications, for example, the soil's ecosystem, Earth's biochemical evolution and origin of life, and drug delivery.[1] The interactions of peptides and proteins with clay surfaces have thus been extensively studied (see ref. 2 and references therein). The adsorption of proteins on clay surfaces is a complex process controlled by various physical and chemical factors, such as cation exchange, electrostatic interactions, hydrophobic affinity, hydrogen bonding and van der Waals forces.[1,2] Clay minerals generally have permanent negative and variable surface charges, thus charged protein molecules can be adsorbed *via* electrostatic interactions, which depend on the negatively and positively charged states of protein molecules in the medium investigated. In addition to cation exchange and electrostatic forces, the hydrophobic (the tetrahedral surface) and hydrophilic' regions (the octahedral surface) on the clay mineral surface are also responsible for both the position and mobility of the water molecules in the halloysite interlayers and on the kaolinite surfaces[3,4] as well as for the adsorption of the hydrophobic protein patches.[1] Hydrophobic interactions are, on the other hand, one of the main forces in the structural stability of proteins in solution.[5] In addition, hydrogen bonding and van der Waal forces are important in the binding of proteins onto clay minerals.[1,6,7]

Both kaolinite and halloysite belong to the kaolinite group of minerals with a similar chemical composition with the nominal formula $Al_2Si_2O_5(OH)_4$ per half unit cell, but with important structural layer-stacking differences.[8] Kaolinite is a naturally-occurring inorganic phyllosilicate with a layer structure consisting of siloxane and gibbsite-like layers.[9] The adsorption sites on kaolinite are located only on the external surface due to their non-expanding layers.[1]

Halloysite forms in volcanic zones, and depending on the variety of crystallization conditions and geological occurrence, halloysite adopts various morphologies such as tubular, spheroidal and plate-like particles, of which the tubular structure is the most common and valuable.[10] Rolled 15–20 alumosilicate sheets of halloysite, named halloysite nanotubes (HNTs), have an ideal formula of $Al_2Si_2O_5(OH)_4 \times nH_2O$, which is similar to kaolinite with additional water between the adjacent layers.[11]

These emerging nanoclays have unique features and innovative uses because their properties and morphologies can be tuned.[12,13] Dried halloysite has a packing periodicity of 0.72 nm

[a]*National Research Council of Italy, C.N.R., Institute of Chemsitry of Organo Metallic Compounds-ICCOM-UOS Pisa, Area di Ricerca, Via G. Moruzzi 1, 56124 Pisa, Italy. E-mail: bramanti@pi.iccom.cnr.it*

[b]*University of Pisa, Dipartimento di Chimica e Chimica Industriale, Via G. Moruzzi 13, 56124 Pisa, Italy*

† Electronic supplementary information (ESI) available. See DOI: 10.1039/c6ra12525e

with hollow lumens (the outside diameter is in the range of 50–100 nm; internal lumen diameter 10–20 nm).[11] A notable feature of halloysite is its different surface chemistry with alumina in the inner (lumen, positively charged up to pH 8.5) and outer sides of the tubes with silicon oxides negatively charged above pH 1.5.[11]

Due to the superior high-temperature-resistant property and their high length/diameter (L/D) ratio, HNTs have been used to produce high-quality ceramics,[14,15] as well as for many other applications, including the loading of biologically active substances and biomolecules, DNA and proteins.[10,16–24] HNTs are considered to be green *i.e.* supposedly not hazardous for the environment, cheap and abundantly naturally available in thousands of tons from natural deposits.[11]

Although no studies have been reported on the effect of the interaction of HNTs with proteins, the interaction of nanoparticles and nanotubes with proteins is actually of interest because of their wide use in biotechnological applications and for the general concern regarding the safety of nanoparticles and the modifications that biological materials may undergo in the human body.[6,25]

Various spectroscopic techniques (NMR, fluorescence, and circular dichroism) are currently used to study protein structural conformations in solution. Fourier Transform Infrared (FTIR) spectroscopy is best suited to compare secondary structures for proteins in solution or adsorbed on a solid support.[25–28] Other methods employed for studying protein adsorption are widely reviewed by Hlady *et al.*[7]

In this work we studied the conformational changes induced by HNTs and Kao on bovine serum albumin (BSA), both in physiological solution (0.9% NaCl) and in ultrapure deionized water by FTIR. BSA is a good 'soft' model protein because it easily undergoes conformational changes upon environment changes.[29]

While nanoparticles are known to interfere with the fibrillation mechanism,[30] to the best of our knowledge, the conformational changes of the BSA induced by its interaction with HNTs have never been investigated. Kao, which has the same composition as HNTs but a different structure, was also investigated as a comparison in order to understand the role of nanostructure morphology. The spectroscopic estimation of the amount of protein adsorbed onto the clays (HNTs or Kao) was also performed.

2. Experimental

Materials, solutions and procedures

BSA (A-8531, EC 232.936.2) was purchased from Aldrich-Sigma-Fluka Chemical Co. (Milan, Italy). Dragonite™ halloysite nanotubes were obtained from Applied Minerals Inc. (New York). HNTs were washed five times with deionized water (18.2 MΩ × cm), using a liquid/solid ratio of 10 mL g^{-1} HNTs. A magnetic stirrer was used to mix each suspension for 1 hour, then the suspension was filtered and dried at 110 °C for 48 hours to eliminate physisorbed water.

Kaolinite (03584) was purchased from Aldrich-Sigma Chemical Co. and used as purchased.

BSA solutions (5.0 and 0.5 mg mL^{-1}) were prepared by dissolving the lyophilized protein in 0.9% NaCl physiological solutions or in ultrapure water (UW). Three different amounts of clay, HNTs or Kao, were added to the BSA solutions in order to have four different clay/BSA ratios: 0, 0.5, 4, 16. It has been reported, infact, that the adsorbed amount of proteins on Kao ranges between 0.04 and 2.5 mg mg^{-1}. This range includes the selected ratios, which correspond to 0.06 (16), 0.25 (4) and 2 mg BSA per mg Kao (0.5).

BSA-clays suspensions were vortexed for one minute and mixed with a magnetic stirrer for one hour. A total of 100 μL of these suspensions were deposited on BaF_2 windows and left to dry in the air for two days. The remaining part of these suspensions were washed three times with the corresponding solvent in order to remove the excess BSA. For each rinsing, the samples were vortexed for 5 min and centrifuged to remove the surnatant. After this, 100 μL of the washed suspensions were deposited on BaF_2 windows and left to dry in the air for two days. For each BSA concentration, the blank was prepared following the same procedure in the absence of HNTs. All dried films were analysed in transmittance mode by FTIR spectroscopy. For several representative samples the FTIR spectra were replicated after 24, 48 and 60 h in order to monitor the drying process. Both the spectrum profiles and the results of spectrum deconvolution did not change after 48 h.

Physiological solution (0.9% NaCl) was purchased from Fresenius Kabi Italia. Ultrapure water prepared with an Elga Purelab-UV system (Veolia Environnement, Paris, France) was used throughout.

Equipment and measurements

Infrared spectra were recorded using a Perkin Elmer Spectrum 100 FTIR spectrophotometer. In order to obtain a suitable S/N ratio, the following spectrometer parameters were used: resolution 4 cm^{-1}, spectra range 450–4000 cm^{-1}, 128 scans. Spectrum software (Perkin-Elmer) and an in-house LabVIEW program for peak fitting were employed to run and process spectra, respectively. The contribution of water vapor is controlled by the Atmospheric Vapor Compensation (AVC) function on the Spectrum™ 100 FT-IR spectrophotometer. This algorithm automatically performs this task in real time addressing the difficult task of reducing the effects of unwanted atmospheric absorptions in sample spectra. The LabVIEW program for peak fitting was based on previous works.[31,32] Prior to curve processing, spectra were normalized in the 1700–1600 cm^{-1} region. This approach was adopted in order to avoid artefacts in absorptions near the limits of the region examined (1700–1600 cm^{-1}). The second derivatives of the amide I band of the spectra examined (1700–1600 cm^{-1} region) were then analysed in order to determine the starting data (number and position of Gaussian components) required for the deconvolution procedure. The choice of the amide I band for structural analysis is due to the very low contribution of the amino acid side chain absorptions present in this region,[33] and to its higher intensity with respect to other amide modes. On the basis of the infrared assignment of amide components, assuming that the

extinction coefficient is the same for all the secondary structures, the secondary structure composition can be obtained from the FTIR spectra. The percentage values of the different secondary structures were estimated by expressing the amplitude value of the bands assigned to each of these structures as a fraction of the total sum of the amplitudes of the amide I components. While the general validity of the above assumption regarding the extinction coefficients remains to be tested, the good correlation found between the secondary structure results obtained by FTIR approaches and X-ray crystallography indicated that this is a reasonable assumption.[31,34]

The spectroscopic estimation of the amount of protein adsorbed onto the clays (HNTs or Kao) was performed on the basis of the amide I optical density of the FTIR non-normalized spectrum recorded before and after the rinsing to remove the excess BSA.

The deconvolution procedure was applied to the amide I band of the FTIR spectra of BSA after rinsing in order to study the conformational changes of BSA adsorbed onto the clay.

The results were reproducible on different films ($N = 3$) and on various area of the same film ($N = 3$). The spectra recorded on $N = 3$ area of the same film were averaged. The deconvolution was performed on the averaged spectrum. The SD bars in Fig. 3, 5 and 6 refer to the data obtained on $N = 3$ different films.

The amount of protein adsorbed by the clays was calculated using the following equation:

$$\%\ \text{protein adsorbed} = \frac{\text{ODr}}{\text{ODnr}} \times 100\ \ \text{(not normalized peak)}$$

where ODr and ODnr are the optical density of the amide I of the non-normalized FTIR spectrum obtained on the dried film from BSA/clay mixture after rinsing the excess BSA or from non-rinsed mixtures, respectively.

3. Results and discussion

BSA (66 500 Da) has 582–607 amino acid residues containing 20 Tyr and 35 cysteine residues, 34 of which are involved in 17 S–S bridge.[35–37] The BSA isoelectric point is 4.7,[38] thus in our operating conditions BSA has a negative charge.

Fig. 1 shows the representative FTIR spectra of BSA, HNTs and Kao. The two characteristic bands of HNTs and Kao at 3696 and 3621 cm^{-1} are due to the stretching vibration of O–H in the inner-surface hydroxyl groups of Al–O–H. The absorption peak at 910 cm^{-1} is likely due to the deformation vibration of the above hydroxyl groups. The presence of the interlayer or adsorbed water is indicated by the stretching vibration at 3450 cm^{-1}.[2] The spectrum of BSA (lyophilized powder) has the characteristic bands of amide A (3282 cm^{-1}), amide B (3056 cm^{-1}), amide I, II, and III (respectively 1642, 1518 and 1234 cm^{-1}). No peaks of HNTs and Kao were present in the range 1700–1250 cm^{-1}. Thus, the study of BSA conformation adsorbed onto the clays was free of interferences.

Fig. 2 shows some representative FTIR spectra of BSA (1740–1475 cm^{-1}), normalized with respect to the amide I region (1700–1600 cm^{-1}) for both HNTs/BSA and Kao/BSA obtained at

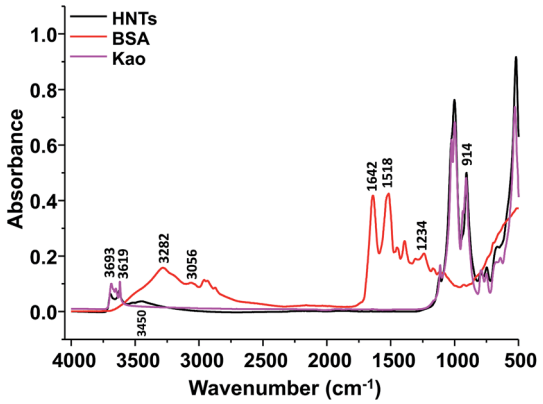

Fig. 1 FTIR spectra of BSA (red line), HNTs (black line), and Kao (pink line).

0 and 0.5 clay/BSA weight ratios and different BSA concentrations (0.5 and 5 mg mL^{-1}) in physiological solution.

Clays interact strongly with BSA. In the case of HNTs/BSA mixtures, the amide I and amide II bands showed more notable differences in terms of frequency shift, and the intensity of the amide I and amide II bands changes compared to Kao/BSA mixtures. This suggests that BSA interacts differently with HNTs than it does with Kao.

The amide II/amide I (AII/AI) ratio is often employed to evaluate changes in the secondary structure of proteins during denaturation.[39–41] This ratio generally increases during denaturation and decreases when peptides increase their ordered structure (beta sheets or helices).

Fig. 3 shows the trend of the AII/AI peak height ratio as a function of the clay/BSA ratio in physiological solution (a) and deionized water (b).

In the case of HNTs/BSA mixtures in physiological solution, we observed a significant decrease in the AII/AI ratio for both 0.5 and 5 mg mL^{-1} BSA as the HNTs/BSA ratio increased. For Kao/BSA mixtures, the trend was the same but the decrease was smaller with respect to pure BSA. The decrease was observed for clay/BSA ratio around 0.5 and was maintained for higher clay/BSA ratio values. Also in ultrapure water, we observed a notable decrease in the AII/AI ratio with the two different BSA concentrations in the case of HNTs/BSA mixtures. In the case of the Kao/BSA mixtures, no significant changes in the AII/AI ratio were observed.

The changes in AII/AI ratio were further investigated in the light of the peak fitting analysis of the BSA amide I band.

Peak fitting procedure for the quantitation of the BSA secondary structure

The curve fitting method applied to the deconvolution of the amide I band of the FTIR spectra was used in order to get detailed information on the secondary structure of BSA, in the tested conditions, on the structural changes induced by clays on BSA and on the percentage of each amide I component.[32]

Fig. 4 shows six representative plots of the curve fitting of the amide I band of BSA at different clay/BSA ratios in physiological solution (panel a) and deionized water (panel b). The quantitative

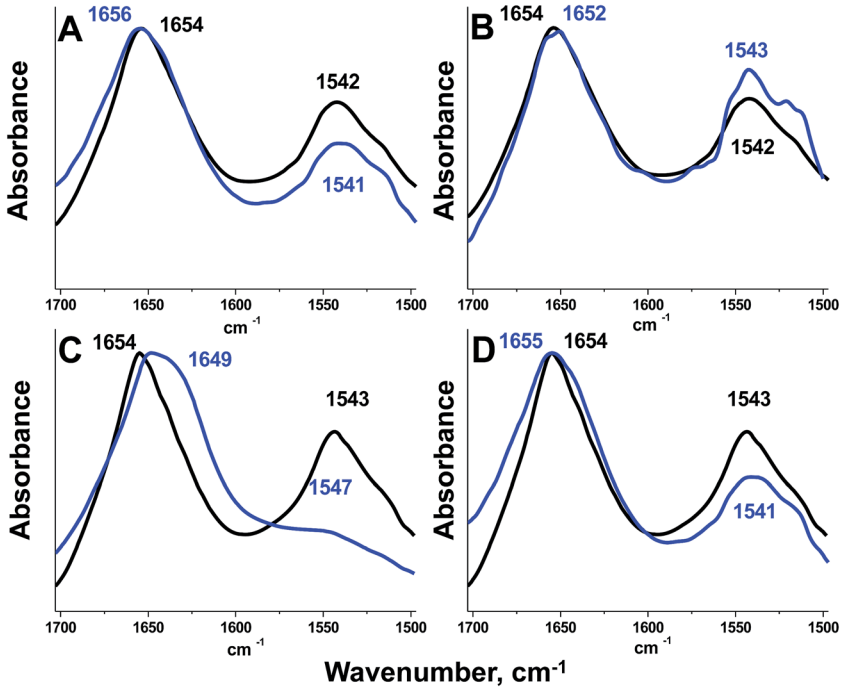

Fig. 2 FTIR normalized spectra in the 1740–1475 cm^{-1} region of clay/BSA mixtures with 0 (black line) and 0.5 (blue line) clay/BSA weight ratios and various BSA concentrations in physiological solution: (A) HNTs/BSA, 0.5 mg mL^{-1} BSA; (B) Kao/BSA, 0.5 mg mL^{-1} BSA; (C) HNTs/BSA, 5 mg mL^{-1} BSA; (D) Kao/BSA, 5 mg mL^{-1} BSA.

results of the secondary structure analysis of BSA in the various conditions investigated are reported in Tables S1–S8 of the ESI.†

Each individual component of amide I was assigned according to the literature,[42,43] namely *ca.* 1690 cm^{-1} (antiparallel β-sheets), *ca.* 1680 cm^{-1} (β turns), and *ca.* 1658 cm^{-1} (α-helix). The band in the 1626–1643 cm^{-1} region was assigned to β-sheets, and the band at 1644–1649 cm^{-1} was assigned to random coil (wide bandwidth) or solvated short helix (narrow bandwidth). The band at 1601–1617 cm^{-1} was assigned to intermolecular β-sheets.

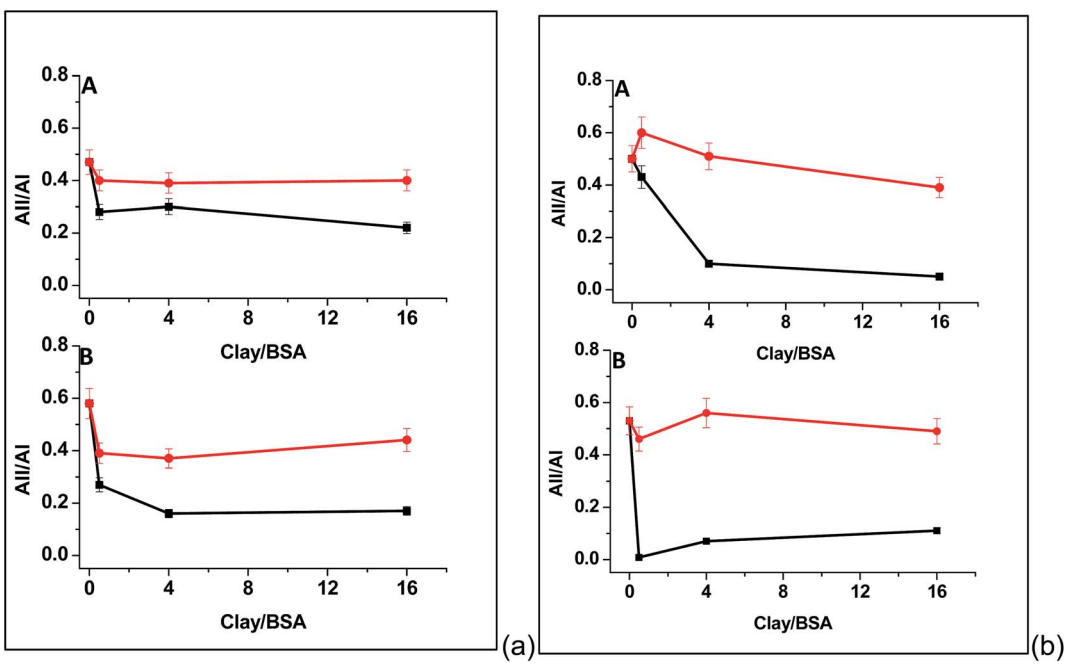

Fig. 3 AII/AI ratio for 0.5 mg mL^{-1} BSA (A) and 5 mg mL^{-1} BSA (B) dissolved in physiological solution (a panel) and deionized water (b panel). HNTs/BSA (black line); Kao/BSA (red line). SD bars refer to FTIR spectra replicates performed on $N = 3$ different films.

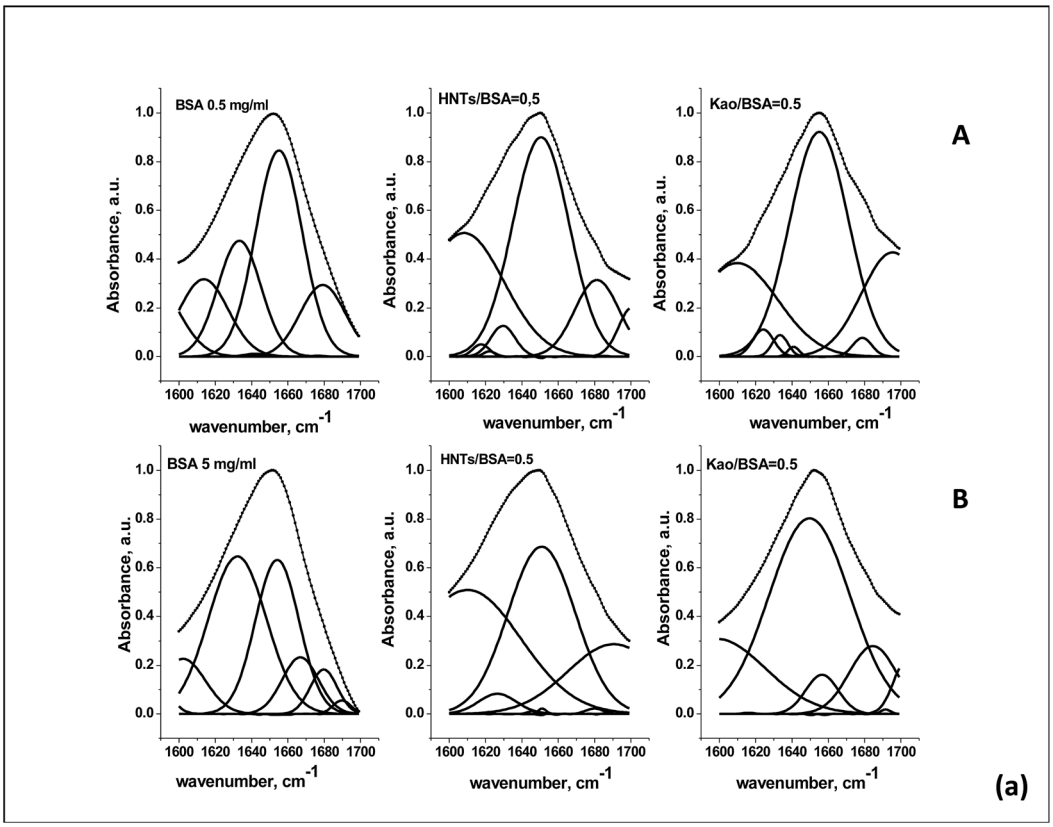

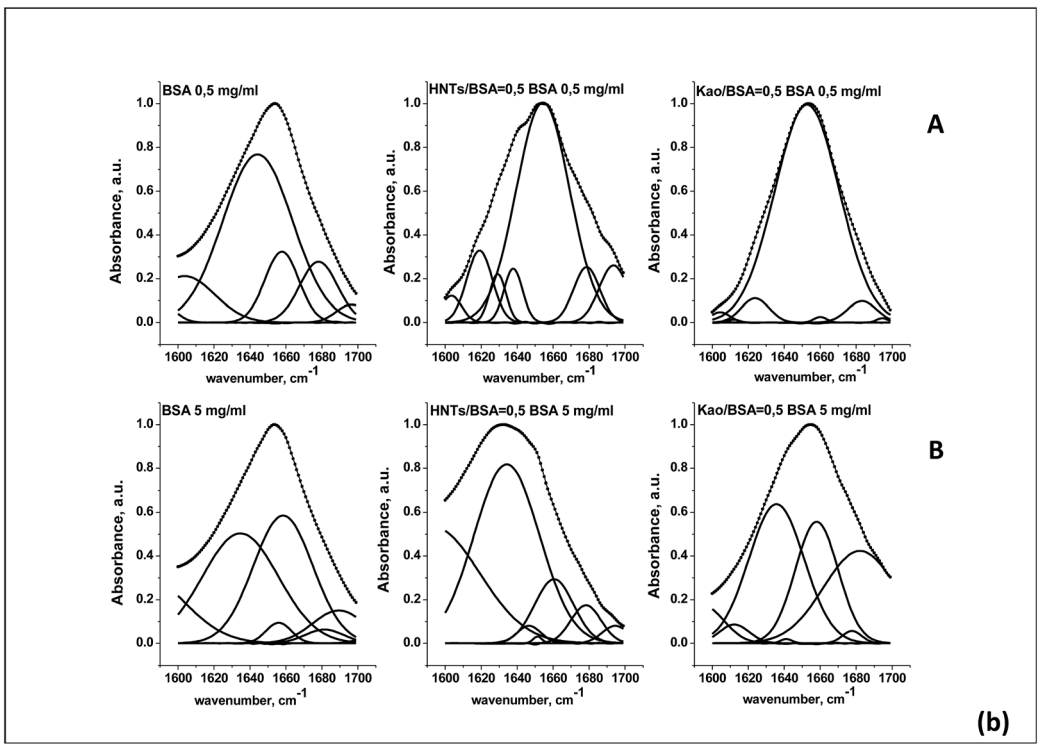

Fig. 4 Curve fitting of the FTIR spectra in the amide I region of 0.5 mg mL^{-1} (panel A) and 5 mg mL^{-1} (panel B) BSA in physiological solution (a) and deionized water (b) (clay/BSA = 0 and 0.5).

Fig. 5 and 6 summarize the percentage variation in the BSA secondary structure components (β-structures, α-helix and random coil), as a function of the clay/BSA ratio. The contribution of β structures is calculated as the sum of the percentages of antiparallel β-sheets, β turns, intramolecular and intermolecular β sheets (Tables S1–S8†). Note that in our

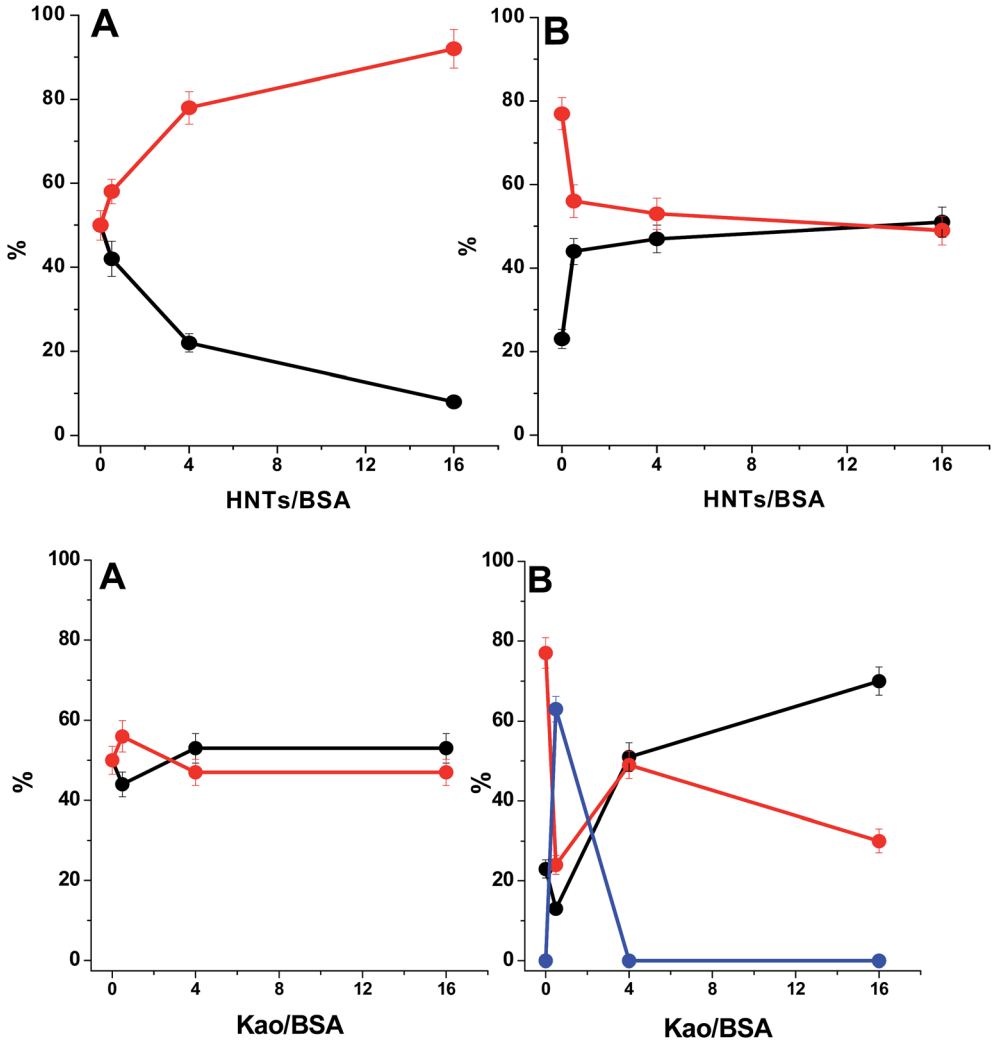

Fig. 5 Secondary structure percentage of BSA as a function of HNTs/BSA and Kao/BSA ratio. (A) 0.5 mg mL^{-1} BSA (B) 5 mg mL^{-1} BSA in physiological solution. β structures (red line); α-helix component (black line); random coil (blue line).

operating conditions the conformational changes observed were related to clay-adsorbed BSA. The excess BSA was, in fact, removed with the rinsing procedure (see Experimental).

Fig. 7A and B show the percentage of adsorbed BSA in the various conditions investigated.

Ionic strength plays a key role in protein conformation, thus BSA in physiological solution and in deionized water adopts a different structure, also in relation to its concentration.

Native BSA (Fig. 5A)

The deconvolution data of 0.5 mg mL^{-1} BSA dissolved in physiological solution (Tables S1 and S2 first column of the ESI†) showed that BSA has a native conformation (about 50% α-helix), according to the literature.[31,44–48] Previous studies performed with FTIR and circular dichroism indicated that native BSA secondary structure contained about 68–50% α-helix and 16–22% β-sheets.

Native BSA interacts with the flat Kao surface keeping its native-like structure (Table S2 of the ESI†). Interestingly, native BSA adsorbed onto HTNs (Table S1 of the ESI†) is almost quantitatively converted into β-sheets. With increasing HNTs/BSA ratio values, we observed a notable decrease in α-helix and an increase in β-structures. At HNTs/BSA ratio > 4, beta structures represented 80% and reached 92% at HNTs/BSA ratio = 16. This result is in agreement with the strong decrease in the AII/AI ratio, and clearly shows that the interaction with the HNTs curved surface induces BSA aggregation.

As the HNTs/BSA ratio increased, however, the amount of adsorbed protein decreased linearly (see Fig. 7 and Table S1 of the ESI†). For higher ratios it is likely that the adsorption of BSA on the surface competes with the clay aggregation process, as well as with the protein aggregation.

The increase in beta structures in the presence of HNTs is in line with previous studies[42,43,49,50] which show the effect of nanoparticles/nanotubes on the protein secondary structure.

Aggregated BSA (Fig. 5B)

A total of 5 mg mL^{-1} BSA dissolved in physiological solution has a 75% beta structure percentage and is likely to be aggregated

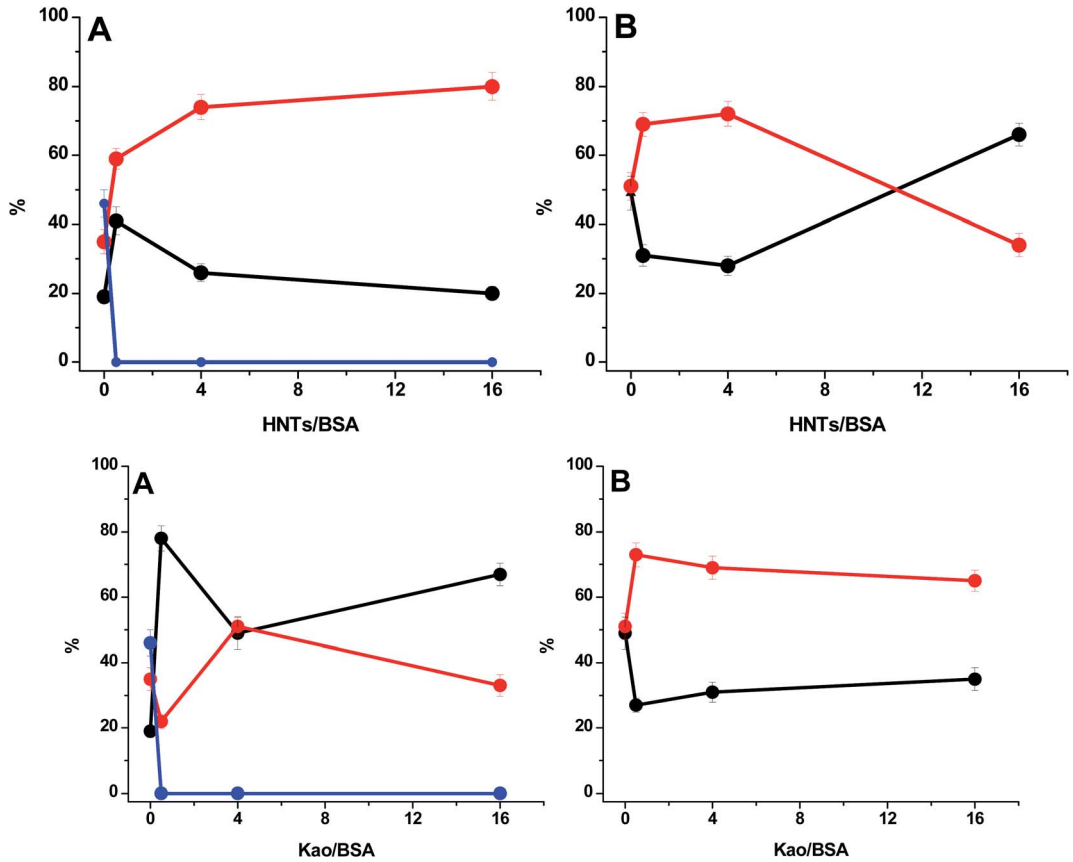

Fig. 6 Secondary structure percentage of BSA as a function of HTNs/BSA and Kao/BSA ratio. (A) 0.5 mg mL^{-1} BSA (B) 5 mg mL^{-1} BSA in deionized water. β structures (red line); α-helix component (black line); random coil (blue line).

(Tables S3 and S4 first column of the ESI†). In fact, the aggregation of BSA seems to proceed through an increased content of β-sheets.[51–53] In a previous work[34] we studied the behaviour of BSA at different pH and temperature conditions. We found that temperature-induced denaturation of BSA was accompanied by the formation of denatured protein molecules and/or small aggregates, rich in β-sheet structures. Campanella *et al.*[54] also found that aggregated BSA is easily obtained in solutions at concentrations of >1 mg mL^{-1}. The seminal observation that an α-helical protein can form β-rich amyloid-like aggregates,

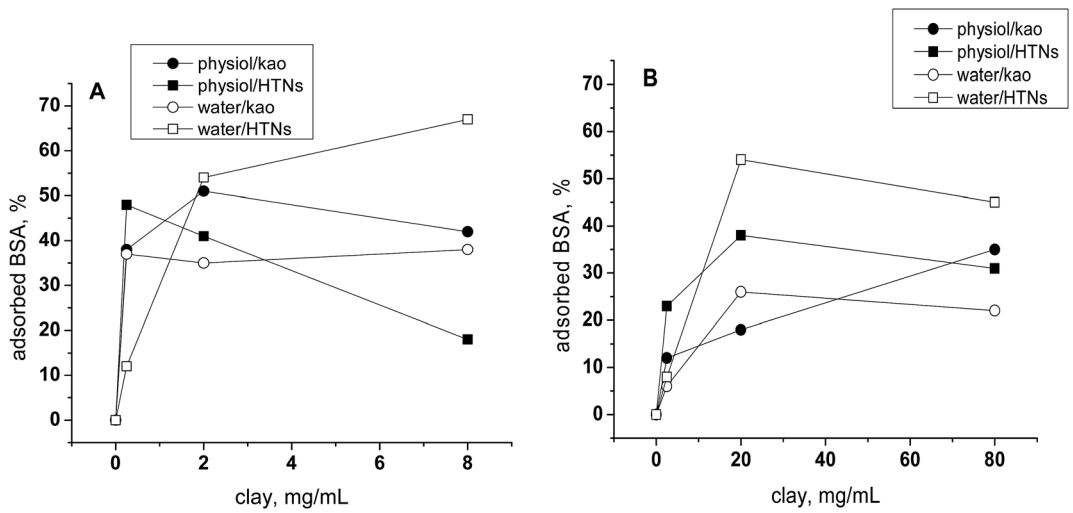

Fig. 7 Percentage of BSA adsorption onto the Kao (circle) and HTNs (square) in physiological solution (filled symbols) and deionized water (open symbols). (A) 0.5 mg mL^{-1} BSA (B) 5 mg mL^{-1} BSA. The coefficient of variation (CV%) is 8–10%.

despite having no predisposition toward β-sheet formation, has generated a lot of interest in recent years.[53,55] An interesting question in this area is how an all α-helical protein transforms into β-rich conformation, in response to a modification in medium conditions, for example, pH, ionic strength, and temperature, thus favouring a partially destabilized state, which ultimately culminates in the formation of amyloid fibril.[56–60]

HNTs and Kao induced notably different conformational changes in 5 mg mL^{-1} BSA, which is aggregated and is characterized by a 75% beta structure.

In the presence of HNTs (Table S3 of the ESI†), we observed a disruption of β-sheets and an increase in α-helix components also at an HNTs/BSA ratio of 0.5. The maximum amount adsorbed was about 35% for HNTs/BSA ratio > 4. Above a HNTs/BSA ratio of 4, the BSA conformation did not change, and α-helix and β-structure percentages reached a plateau (about 50% α-helix and 50% β-structures). In the HNTs/BSA mixtures, no disordered structures (random coil) were observed.

Also the interaction of aggregated BSA with Kao disrupts β structures (Table S4 of the ESI†). However, at low Kao/BSA ratios (=0.5) β structures were converted into random coils. Only at higher Kao/BSA (>4) ratios, were random coils converted into α-helices and β structures. For the Kao/BSA = 16 ratio, the helix component increased and β structures decreased. In this case the amount of adsorbed BSA increased linearly with the Kao/BSA ratio.

Random BSA (Fig. 6A)

The conformation of BSA dissolved in deionized water is very different compared to when dissolved in a physiological solution (Tables S5 and S6 first column of the ESI†). At 0.5 mg mL^{-1} concentration, BSA has a high percentage of disordered structures (46% random coil, 13% intermolecular β-sheets, 19% α-helix, 17% β-turns, and 5% anti parallel β-sheets).

We found that the interaction of HNTs and Kao with "random" BSA led to the quantitative conversion of 48% random coil into ordered structures: HNTs into β-sheets (Table S5 of the ESI†), and Kao into α-helix (Table S6 of the ESI†). Unfolded BSA adsorbed onto HNTs had an almost 80% β-sheet conformation and reached almost 70% of protein adsorbed as the HNTs/BSA ratio increased. The same unfolded species interacted with the flat surface of Kao promoting an NL structure and about 35% of adsorbed protein.

Native-like BSA (Fig. 6B)

Unexpectedly, in deionized water at 5 mg mL^{-1} BSA has a native-like form (49% helix and 51% β structures) (Tables S7 and S8 first column of the ESI†). The basic and acid side chains of protein amino acids likely act as a buffer.[61]

HNTs induced on adsorbed BSA a decrease in the helix component and an increase in β-structures up to about 72% at HNTs/BSA = 4 (Table S7 of the ESI†). For higher ratios, β-sheets were converted again into α-helix (about 66% at HNTs/BSA = 16 ratio). The adsorption was the maximum (more than 50%) at around HNTs/BSA ratio = 4, in relation to the maximum percentage of beta structures.

Kao induced a decrease in the helix component of adsorbed BSA and an increase of β-structure up to 70%, with a plateau between 0.5 and Kao/BSA ratio = 16 (Table S8 of the ESI†). Only 25% BSA was adsorbed onto Kao.

Table 1 summarizes the BSA conformational changes induced by the clays in all the conditions explored.

The data show that the effect of the interactions of BSA with clays is very different depending on the initial structure of the protein and on the clay morphology. In response to changing conditions, BSA molecules show a large conformational adaptability.[35,62] Protein adsorption is the first event that occurs when a material is introduced into a physiological fluid, because proteins have a high affinity for surfaces. Both the surface chemistry of the material (*e.g.* nanoparticles) and the protein intrinsic stability govern protein adsorption and, thus, the final protein conformation. Thus, adsorption may occur with few structural changes or cause denaturation also in relation to the character of the surface.

The conformational changes described above suggest that the different hydrophobicity, as well as the electrostatic attraction of the protein may be responsible for the differences in the adsorption curves. All these interactions are different depending on the protein conformational state: native, native-like, aggregated, random coiled. An adsorbent surface can "compete" for the same interactions and minimize the total free energy of the system by changing the protein structure. Thus, the adsorption process may result in a surface-induced protein denaturation/rearrangement.[63] It is known that clay mineral surfaces can have a denaturing effect on adsorbed proteins for two reasons: (i) they are dehydrating agents, because they perturb the random environment of water molecules that globular proteins need to maintain their native structure; and (ii) clay surfaces can establish non-bonded interactions with proteins

Table 1 BSA conformational changes induced by clays in all the conditions explored. N = native, NL = native like, R = random, A = aggregated BSA, α = α-helix and β = β-structures

Solvent	BSA concentration (mg mL^{-1})	Secondary structure conformational changes induced by clays	
		HTNs	Kao
Physiological solution	0.5	N → β (92%)	N → NL
Physiological solution	5	A (80% β) → NL (51% α)	A (80% β) → R (63%) → NL (70% α)
Bidistilled water	0.5	48% R → 80% β	48% R → NL (49% α) → NL (67% α)
Bidistilled water	5	NL (51% α) → 72% β → NL (66% α)	NL (51% α) → 69% β

which compete effectively with the interactions inside a peptide chain. The changes in the secondary and tertiary protein structures induced by adsorption to clay surfaces lead to backbone torsion.[64]

In our operating conditions, the HNT and Kao outer surfaces have a negative charge. Thus, the surface interaction may be due to the positive groups (such as arginine, glutamine, lysine, histidine, as well as amino terminal groups) of the protein. In addition to electrostatic interactions, also hydrophobic interactions and structural changes of the protein molecules may be the driving forces for the adsorption process of BSA.[65] In several cases the adsorption-induced structural rearrangement has been found to result in a higher thermostability of the adsorbed protein.[66]

A previous FTIR analysis of the interaction of BSA with montmorillonite showed an extensive pH independent unfolding of BSA related to new orientations of the positively charged Lys and Arg residues which are forced to move close to the negative clay surface.[67] In this work the interaction with Kao did not lead to significant conformational changes in native BSA. However, Kao induced the disruption of aggregated species through a random coil and the subsequent α-helix formation.

Other studies on the interaction of nanoparticles/nanotubes with BSA have shown a partial unfolding of protein in the presence of gold, diamond and carbon nanoparticles and carbon nanotubes.[42,43,49,50] Previous studies have shown the effect of nanoparticles on amyloid aggregation.[68–70]

Cabaleiro-Lago *et al.* observed that in protein mutants with a high intrinsic stability and low intrinsic aggregation rate, nanoparticles accelerated the amyloid fibril formation. In protein mutants with a low intrinsic stability and high intrinsic aggregation rate, nanoparticles showed the opposite behaviour and led to a delay in amyloid fibril formation.[69]

In this work, HNTs in native BSA in physiological solution induced a misfolding with a decrease in the α-helix and an increase in β structures, as well as the conversion of random BSA

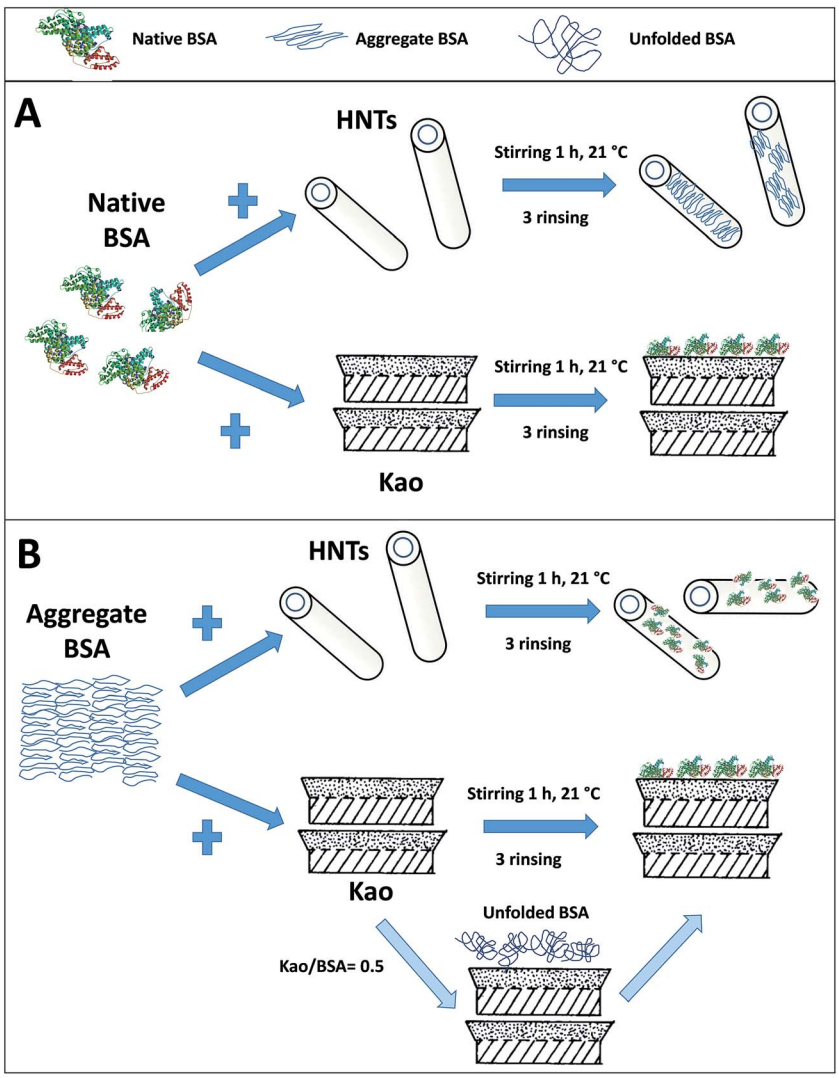

Fig. 8 Conformational changes induced by the interactions between clays and BSA in physiological solution. 0.5 mg mL^{-1} BSA (A); 5 mg mL^{-1} BSA (B).

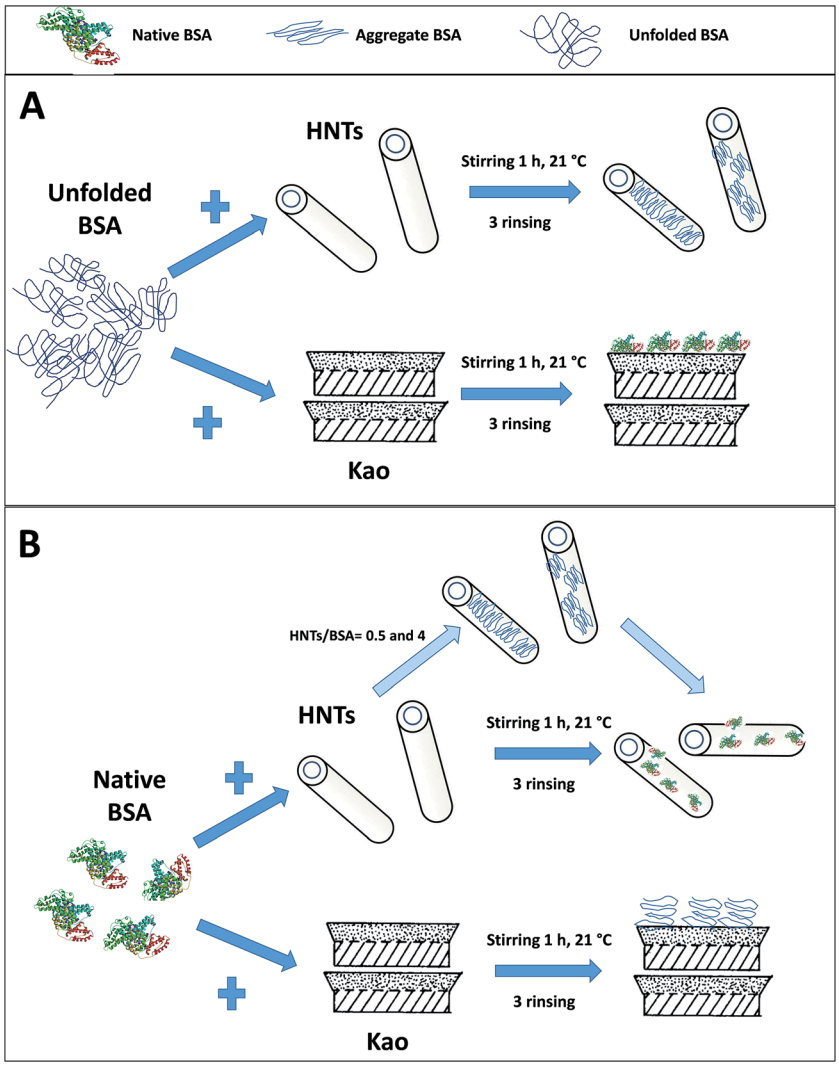

Fig. 9 Conformational changes induced by the interactions between clays and BSA in deionized water. 0.5 mg mL^{-1} BSA (A); 5 mg mL^{-1} BSA (B).

in water into β structures, which would seem to indicate protein aggregation. Previous studies have shown the aggregation of proteins in the presence of gold and silica nanoparticles.[71,72] In these studies nanoparticles acted as a nucleation centre for protein aggregation. On the other hand, HNTs interacted with aggregated BSA inducing the conversion β → α.

The involvement of HNTs in the process of the α/β conversion of BSA is a totally new finding and suggests the possible involvement of nanostructures in protein fibril formation, *i.e.* in the process that converts protein monomers into fibrils and *vice versa*. The increase in beta structures observed in the presence of HNTs is in line with previous studies.[42,43,49,50]

According to the data reported in Table S3,† intermolecular β sheets appear only at HNTs/BSA ratio = 0.5, which corresponds to 2 mg BSA per mg HTNs (*i.e.* a weight excess of protein). Considering that 5 mg mL^{-1} BSA is an aggregating concentration, intermolecular β sheets may be justified by the fact that the tubular clay is not enough to interfere with aggregated, very stable species.

By increasing HTNs we can hypothesize that HTNs surface competes with aggregation and BSA molecules adsorbed onto HTNs have the significant conformational changes described in Table S3.†

From the inspection of data reported in Table S4† it is also notable that the appearance of intermolecular β sheets corresponds to a high value of the ratio (16, *i.e.* 0.06 mg BSA per mg Kao) and the random coil at low value (0.5). We can hypothesize that when the protein is scarce the BSA adsorbed has enough space to "smear" onto the flat Kao surface and it keeps/maintains a moderate percentage of antiparallel β sheets (1620 and 1692 cm^{-1} components).

When the Kao/BSA ratio = 0.5 (*i.e.* 2 mg BSA per mg Kao, a weight excess of protein) we can hypothesize that Kao is able to interfere with aggregated BSA. However, BSA molecules have not enough space on the Kao flat surface to arrange in an ordered structure.

As far as random BSA concerns (Tables S5 and S6†), random coil is a very unstable structure and the interaction of BSA with

both HTNs and Kao surfaces induces more stable, ordered structures.

The amount of BSA adsorbed onto clays is in agreement with the values found by other authors (ref. 1 and references therein). We found that the adsorption in water is, in general, higher than in physiological solution, in agreement with the literature data.[6,73] The ionic strength affects the adsorption of protein on clay minerals because increasing ion strength leads to a competitive ion exchange in the case of electrostatic adsorption. However, salt ions may compete for hydration protein water, thereby causing the exposure of the hydrophobic groups of protein, and leading to an increase in the hydrophobic interactions and, consequently, of the adsorption.[74]

Many studies have demonstrated that the surface curvature plays a key role in the adsorption mechanism and that the amount of the protein's perturbed secondary structure is influenced strongly by different degrees of curvature. For a specific protein, a highly curved nanoscale surface can reduce or promote the retention of the native protein structure in comparison to macroscopic "flat" supports.[75–81]

In an aqueous solution, the natural nanotubular clays do not possess a dispersed structure but an aggregated form.[82] It is possible that, in several conditions, the interaction with BSA favours the dispersion of HNTs; whereas in excess of HNTs, clay–clay aggregation is not favoured.

Fig. 8 and 9 show the results of BSA conformational changes.

4. Conclusions

FTIR spectroscopy is a well-established experimental technique for studying the secondary structure of proteins. The main advantage of FTIR over other techniques is convenience, as protein spectra can be obtained in a wide range of environments, including heterogeneous systems, with a small amount of sample.

In this study, FTIR spectroscopy provided novel information on the BSA secondary structure in physiological solution and in deionized water. Depending on the conditions investigated, in the absence of salting-in or salting-out agents, BSA adopted a native/native-like structure, an aggregated structure or a random coil-rich conformation.

FTIR enabled us to investigate the structural changes of BSA conformers induced by the surface interactions with clays (tubular HNTs or flat Kao) and to estimate the amount of adsorbed protein onto clays. The FTIR analysis of the interaction of BSA with these clays showed an extensive modification of the BSA secondary structure due to the adsorption, confirming that BSA is a "soft" protein.

In physiological solution, the curved nanoscale surface of HNTs promoted the almost quantitative conversion of native BSA into a beta structure. Aggregated BSA interacted with the curved nanoscale surface of HNTs thereby promoting the formation onto the surface of NL BSA. By interacting with the flat Kao surface, instead, both native and aggregated BSA kept the native-like (NL) structure.

In deionized water HNTs induced beta sheets in the NL structure of BSA, and for higher HNTs/BSA ratios, the NL structure increased its α-helix content. NL BSA in deionized water produced beta structures onto the flat surface of Kao. Unfolded BSA adsorbed onto HNTs gave beta sheets, while the flat surface of Kao promoted an NL structure in adsorbed BSA.

All these results demonstrated that the surface curvature radius plays a key role in the final conformation, interfering profoundly with the α/β transitions of BSA. This could have potential applications in the study of protein misfolding/aggregation, and these materials could also be used in analytical chemistry for protein purification.

It is possible that *in vivo* HTNs – and, in general, nanostructures – may alter the transport properties of BSA in various biological processes.

Acknowledgements

This work was supported by the projects FIRB 2012 (No. RBFR12ETL5), funded by the Italian Ministry of University and Research, and PRA_2016_46 funded by the University of Pisa.

References

1 W. H. Yu, N. Li, D. S. Tong, C. H. Zhou, C. X. Lin and C. Y. Xu, *Appl. Clay Sci.*, 2013, **80–81**, 443–452.
2 R. Duarte-Silva, M. A. Villa-Garcia, M. Rendueles and M. Diaz, *Appl. Clay Sci.*, 2014, **90**, 73–80.
3 D. Presti, A. Pedone, G. Mancini, C. Duce, M. R. Tine and V. Barone, *Phys. Chem. Chem. Phys.*, 2016, **18**, 2164–2174.
4 C. Duce, S. Vecchio Ciprioti, L. Ghezzi, V. Ierardi and M. R. Tinè, *J. Therm. Anal. Calorim.*, 2015, **121**, 1011–1019.
5 R. D. Tilton, C. R. Robertson and A. P. Gast, *Langmuir*, 1991, **7**, 2710–2718.
6 W. H. Yu, N. Li, D. S. Tong, C. H. Zhou, C. X. Lin and C. Y. Xu, *Appl. Clay Sci.*, 2013, **80–81**, 443–452.
7 V. Hlady, J. Buijs and H. P. Jennissen, *Methods Enzymol.*, 1999, **309**, 402–429.
8 Z. Rozynek, T. Zacher, M. Janek, M. Čaplovičová and J. O. Fossum, *Appl. Clay Sci.*, 2013, **77–78**, 1–9.
9 H. F. Cheng, Q. F. Liu, J. Yang, S. J. Ma and R. L. Frost, *Thermochim. Acta*, 2012, **545**, 1–13.
10 M. Du, B. Guo and D. Jia, *Polym. Int.*, 2010, **59**, 574–582.
11 Y. Lvov and E. Abdullayev, *Prog. Polym. Sci.*, 2013, **38**, 1690–1719.
12 G. Cavallaro, D. I. Donato, G. Lazzara and S. Milioto, *J. Phys. Chem. C*, 2011, **115**, 20491–20498.
13 Y. Lvov, W. Wang, L. Zhang and R. Fakhrullin, *Adv. Mater.*, 2016, **28**, 24.
14 C. Viti, M. Lupieri and M. Reginelli, *Neues Jahrb. Mineral., Abh.*, 2007, **183**, 203–213.
15 I. R. Wilson, *Clay Miner.*, 2004, **39**, 1–15.
16 Y. M. Lvov, D. G. Shchukin, H. Möhwald and R. R. Price, *ACS Nano*, 2008, **2**, 814–820.
17 E. Abdullayev and Y. Lvov, *J. Nanosci. Nanotechnol.*, 2011, **11**, 10007–10026.
18 Y. J. Suh, D. S. Kil, K. S. Chung, E. Abdullayev, Y. M. Lvov and D. Mongayt, *J. Nanosci. Nanotechnol.*, 2011, **11**, 661–665.

19 A. Joshi, E. Abdullayev, A. Vasiliev, O. Volkova and Y. Lvov, *Langmuir*, 2013, **29**, 7439–7448.
20 E. Abdullayev and Y. Lvov, *J. Mater. Chem.*, 2010, **20**, 6681–6687.
21 Y. M. Lvov, N. G. Veerabadran and R. R. Price, *Nano*, 2007, **02**, 115–120.
22 N. G. Veerabadran, D. Mongayt, V. Torchilin, R. R. Price and Y. M. Lvov, *Macromol. Rapid Commun.*, 2009, **30**, 99–103.
23 D. G. Shchukin, G. B. Sukhorukov, R. R. Price and Y. M. Lvov, *Small*, 2005, **1**, 510–513.
24 M. H. Shamsi and K. E. Geckeler, *Nanotechnology*, 2008, **19**, 075604.
25 A. Bouhekka and T. Bürgi, *Appl. Surf. Sci.*, 2012, **261**, 369–374.
26 A. Barth, *Biochim. Biophys. Acta, Bioenerg.*, 2007, **1767**, 1073–1101.
27 A. Barth and C. Zscherp, *Q. Rev. Biophys.*, 2002, **35**, 369–430.
28 A. Barth and P. I. Haris, *Biological and Biomedical Infrared Spectroscopy*, IOS Press, Amsterdam, Netherlands, 2009.
29 K. Nakanishi, T. Sakiyama and K. Imamura, *J. Biosci. Bioeng.*, 2001, **91**, 233–244.
30 S. D. Luthuli, M. M. Chili, N. Revaprasadu and A. Shonhai, *IUBMB Life*, 2013, **65**, 454–461.
31 E. Bramanti and E. Benedetti, *Biopolymers*, 1996, **38**, 639–653.
32 E. Bramanti, M. Bramanti, P. Stiavetti and E. Benedetti, *J. Chemom.*, 1994, **8**, 409–421.
33 Y. N. Chirgadze, O. V. Fedorov and N. P. Trushina, *Biopolymers*, 1975, **14**, 679–694.
34 E. Bramanti, C. Ferrari, V. Angeli, M. Onor and R. E. Synovec, *Talanta*, 2011, **85**, 2553–2561.
35 D. C. Carter and J. X. Ho, *Adv. Protein Chem.*, 1994, **45**, 153–203.
36 J. R. Brown, T. Low, P. Beherns, P. Sepulved, K. Parker and E. Blakeney, *Fed. Proc.*, 1971, 1241–1245.
37 K. Hirayama, S. Akashi, M. Furuya and K.-I. Fukuhara, *Biochem. Biophys. Res. Commun.*, 1990, **173**, 639–646.
38 K. M. Pierce, E. Bramanti, M. Onor, R. Spiniello, A. Kangas, K. J. Skogerboe and R. E. Synovec, *Talanta*, 2010, **80**, 1445–1451.
39 T. J. Lenk, B. D. Ratner, R. M. Gendreau and K. K. Chittur, *J. Biomed. Mater. Res.*, 1989, **23**, 549–570.
40 K. Kato, T. Matsui and S. Tanaka, *Appl. Spectrosc.*, 1987, **41**, 861–865.
41 E. Bramanti, F. Lenci and A. Sgarbossa, *Eur. Biophys. J.*, 2010, **39**, 1493–1501.
42 X. Shi, D. Li, J. Xie, S. Wang, Z. Wu and H. Chen, *Chin. Sci. Bull.*, 2012, **57**, 1109–1115.
43 H. D. Wang, C. H. Niu, Q. Q. Yang and I. Badea, *Nanotechnology*, 2011, **22**, 145703.
44 S. Cai and B. R. Singh, *Biophys. Chem.*, 1999, **80**, 7–20.
45 Y. H. Chen, J. T. Yang and K. H. Chau, *Biochemistry*, 1974, **13**, 3350–3359.
46 J. F. Foster, in *Albumin: Structure, Function and Uses*, ed. V. M. R. O. A. Rothschild, Pergamon, 1977, pp. 53–84, DOI: 10.1016/b978-0-08-019603-9.50010-7.
47 R. G. Reed, R. C. Feldhoff, O. L. Clute and T. Peters Jr, *Biochemistry*, 1975, **14**, 4578–4583.
48 I. Sjoholm and I. Ljungstedt, *J. Biol. Chem.*, 1973, **248**, 8434–8441.
49 S. Mandal, M. Hossain, P. S. Devi, G. S. Kumar and K. Chaudhuri, *J. Hazard. Mater.*, 2013, **248–249**, 238–245.
50 L. Li, R. Lin, H. He, L. Jiang and M. Gao, *Spectrochim. Acta, Part A*, 2013, **105**, 45–51.
51 N. K. Holm, S. K. Jespersen, L. V. Thomassen, T. Y. Wolff, P. Sehgal, L. A. Thomsen, G. Christiansen, C. B. Andersen, A. D. Knudsen and D. E. Otzen, *Biochim. Biophys. Acta, Proteins Proteomics*, 2007, **1774**, 1128–1138.
52 S. M. Vaiana, A. Emanuele, M. B. Palma-Vittorelli and M. U. Palma, *Proteins: Struct., Funct., Bioinf.*, 2004, **55**, 1053–1062.
53 M. Bhattacharya, N. Jain and S. Mukhopadhyay, *J. Phys. Chem. B*, 2011, **115**, 4195–4205.
54 B. Campanella, M. Onor, A. D'Ulivo, S. Giannarelli and E. Bramanti, *Anal. Chem.*, 2014, **86**, 2251–2256.
55 M. Fändrich, V. Forge, K. Buder, M. Kittler, C. M. Dobson and S. Diekmann, *Proc. Natl. Acad. Sci. U. S. A.*, 2003, **100**, 15463–15468.
56 J. Juárez, S. G. López, A. Cambón, P. Taboada and V. Mosquera, *J. Phys. Chem. B*, 2009, **113**, 10521–10529.
57 J. Juárez, P. Taboada and V. Mosquera, *Biophys. J.*, 2009, **96**, 2353–2370.
58 N. J. M. Sanghamitra, N. Varghese and C. N. R. Rao, *Chem. Phys. Lett.*, 2010, **496**, 104–108.
59 V. Vetri, F. Librizzi, M. Leone and V. Militello, *Eur. Biophys. J.*, 2007, **36**, 717–725.
60 Y. Wei, L. Chen, J. Chen, L. Ge and R. He, *BMC Cell Biol.*, 2009, **10**, 10.
61 H. N. Christensen, *Ann. N. Y. Acad. Sci.*, 1966, **133**, 34–40.
62 T. Peters Jr, *Adv. Protein Chem.*, 1985, **37**, 161–245.
63 V. Hlady, J. Buijs and H. P. Jennissen, in *Methods in Enzymology*, Academic Press, 1999, vol. 309, pp. 402–429.
64 C. H. Yu, M. A. Norman, S. Q. Newton, D. M. Miller, B. J. Teppen and L. Schafer, *J. Mol. Struct.*, 2000, **556**, 95–103.
65 W. Norde, in *Surfactant Science Series*, ed. M. E. Malmsten, Marcel Dekker, New York, 1998, vol. 75, p. 27.
66 T. Vermonden, C. E. Giacomelli and W. Norde, *Langmuir*, 2001, **17**, 3734–3740.
67 S. Servagent-Noinville, M. Revault, H. Quiquampoix and M. H. Baron, *J. Colloid Interface Sci.*, 2000, **221**, 273–283.
68 C. Cabaleiro-Lago, I. Lynch, K. A. Dawson and S. Linse, *Langmuir*, 2010, **26**, 3453–3461.
69 C. Cabaleiro-Lago, O. Szczepankiewicz and S. Linse, *Langmuir*, 2012, **28**, 1852–1857.
70 A. M. Saraiva, I. Cardoso, M. C. Pereira, M. A. N. Coelho, M. J. Saraiva, H. Mohwald and G. Brezesinski, *ChemBioChem*, 2010, **11**, 1905–1913.
71 S. Rocha, A. F. Thünemann, M. d. C. Pereira, M. Coelho, H. Möhwald and G. Brezesinski, *Biophys. Chem.*, 2008, **137**, 35–42.
72 D. M. Zhang, O. Neumann, H. Wang, V. M. Yuwono, A. Barhoumi, M. Perham, J. D. Hartgerink, P. Wittung-Stafshede and N. J. Halas, *Nano Lett.*, 2009, **9**, 666–671.

73 K. Ralla, U. Sohling, D. Riechers, C. Kasper, F. Ruf and T. Scheper, *Bioprocess Biosyst. Eng.*, 2010, **33**, 847–861.
74 T. Simonson and C. L. Brooks, *J. Am. Chem. Soc.*, 1996, **118**, 8452–8458.
75 M. Lundqvist, I. Sethson and B.-H. Jonsson, *Langmuir*, 2004, **20**, 10639–10647.
76 W. Shang, J. H. Nuffer, J. S. Dordick and R. W. Siegel, *Nano Lett.*, 2007, **7**, 1991–1995.
77 W. Shang, J. H. Nuffer, V. A. Muniz-Papandrea, W. Colon, R. W. Siegel and J. S. Dordick, *Small*, 2009, **5**, 470–476.
78 P. Roach, D. Farrar and C. C. Perry, *J. Am. Chem. Soc.*, 2006, **128**, 3939–3945.
79 A. A. Vertegel, R. W. Siegel and J. S. Dordick, *Langmuir*, 2004, **20**, 6800–6807.
80 H. S. Mandal and H. B. Kraatz, *J. Am. Chem. Soc.*, 2007, **129**, 6356–6357.
81 Q. X. Mu, W. Liu, Y. H. Xing, H. Y. Zhou, Z. W. Li, Y. Zhang, L. H. Ji, F. Wang, Z. K. Si, B. Zhang and B. Yan, *J. Phys. Chem. C*, 2008, **112**, 3300–3307.
82 H. Lun, J. Ouyang and H. Yang, *RSC Adv.*, 2014, **4**, 44197–44202.